Behavioral/Systems/Cognitive

NADPH Oxidase-Dependent Regulation of T-Type Ca^{2+} Channels and Ryanodine Receptors Mediate the Augmented Exocytosis of Catecholamines from Intermittent Hypoxia-Treated Neonatal Rat Chromaffin Cells

Dangjai Souvannakitti,[1] Jayasri Nanduri,[1] Guoxiang Yuan,[1] Ganesh K. Kumar,[1] Aaron P. Fox,[2] and Nanduri R. Prabhakar[1]

The Center for Systems Biology of O_2 Sensing, Departments of [1]Medicine and [2]Neurobiology, Pharmacology, and Physiology, University of Chicago, Chicago, Illinois 60637

Nearly 90% of premature infants experience the stress of intermittent hypoxia (IH) as a consequence of recurrent apneas (periodic cessation of breathing). In neonates, catecholamine secretion from the adrenal medulla is critical for maintaining homeostasis under hypoxic stress. We recently reported that IH treatment enhanced hypoxia-evoked catecholamine secretion and $[Ca^{2+}]_i$ responses in neonatal rat adrenal chromaffin cells and involves reactive oxygen species (ROS). The purpose of the present study was to identify the source(s) of ROS generation and examine the mechanisms underlying the enhanced catecholamine secretion by IH. Neonatal rats of either sex (postal day 0–5) were exposed to either IH or normoxia. IH treatment increased NADPH oxidase (NOX) activity, upregulated NOX2 and NOX4 transcription in adrenal medullae, and a NOX inhibitor prevented the effects of IH on hypoxia-evoked chromaffin cell secretion. IH upregulated Cav3.1 and Cav3.2 T-type Ca^{2+} channel mRNAs via NOX/ROS signaling and augmented T-type Ca^{2+} current in IH-treated chromaffin cells. Mibefradil, a blocker of T-type Ca^{2+} channels attenuated the effects of hypoxia on $[Ca^{2+}]_i$ and catecholamine secretion in IH-treated cells. In Ca^{2+}-free medium, IH-treated cells exhibited higher basal $[Ca^{2+}]_i$ levels and more pronounced $[Ca^{2+}]_i$ responses to hypoxia compared with controls, and blockade of ryanodine receptors (RyRs) prevented these effects. RyR2 and RyR3 mRNAs were upregulated, RyR2 was S-glutathionylated in IH-treated adrenal medullae, and NOX/ROS inhibitors prevented these effects. These results demonstrate that neonatal IH treatment leads to NOX/ROS-dependent recruitment of T-type Ca^{2+} channels and RyRs, resulting in augmented $[Ca^{2+}]_i$ mobilization and catecholamine secretion.

Introduction

Catecholamine (CA) secretion from the adrenal medulla is critical for maintaining homeostasis under hypoxia. The role of adrenal medulla is especially critical in neonatal life, wherein sympathetic innervation to the target organs is incomplete (Lagercrantz and Bistoletti, 1977; Seidler and Slotkin, 1985). Seventy to ninety percent of prematurely born neonates experience the stress of intermittent hypoxia (IH) as a consequence of breathing disorders manifested as recurrent apneas (Stokowski, 2005). We reported recently that adrenal chromaffin cells from neonatal rat pups treated with IH from postnatal day 0 (P0) to P5 exhibit marked enhancement of hypoxia-evoked catecholamine secretion and pronounced elevations in $[Ca^{2+}]_i$ (Souvannakitti et al., 2009). Antioxidant treatment completely prevented chromaffin cell responses to IH, suggesting the involvement of reactive oxygen species (ROS) signaling. Neither the source(s) nor the mechanism (s) by which ROS signaling affects catecholamine secretion and $[Ca^{2+}]_i$ changes in IH-treated chromaffin cells were examined.

The family of NADPH oxidases (NOX) constitutes one of the major sources of ROS generation in mammalian cells (for references, see Bedard and Krause, 2007). IH treatment upregulates NOX isoforms in the peripheral nervous system (Peng et al., 2009) and the CNS of rodents (Zhan et al., 2005), as well as in PC12 cells (Yuan et al., 2008). Activation of NOX and the ensuing generation of ROS mediate systemic responses to IH, including the sensory long-term facilitation of carotid bodies (Peng et al., 2009) and altered sleep behavior in rodents (Zhan et al., 2005). These observations prompted us to examine whether ROS generated by NOX mediate the augmented catecholamine secretion and $[Ca^{2+}]_i$ changes in neonatal adrenal chromaffin cells treated with IH.

Hypoxia-evoked catecholamine secretion from adrenal chromaffin cells is mediated by Ca^{2+} influx via voltage-gated Ca^{2+} channels (Mochizuki-Oda et al., 1997). A recent study on neona-

Received May 5, 2010; revised June 14, 2010; accepted June 17, 2010.

The work was supported by National Institutes of Health/National Heart, Lung, and Blood Institute Grants HL-90554, HL-76537, HL-86493 (N.R.P.), HL-089616 (G.K.K.), and GM-081809, a Philip Morris International grant (A.P.F.), and an American Heart Association predoctoral fellowship (D.S.). We thank Prof. E. Carbone for helpful suggestions for this manuscript.

Correspondence should be addressed to Nanduri R. Prabhakar, The Center for Systems Biology of O_2 Sensing, Department of Medicine, The University of Chicago, MC 5068, 5841 S. Maryland Avenue, Chicago, IL 60637. E-mail: nanduri@uchicago.edu.

DOI:10.1523/JNEUROSCI.2307-10.2010

 0270-6474/10/3010763-10$15.00/0

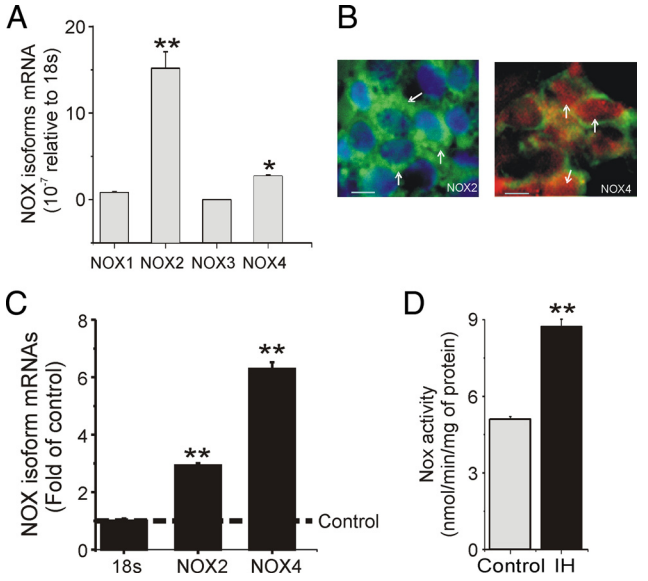

Figure 1. IH upregulates NOX mRNAs and NOX activity in neonatal adrenal medullae. ***A***, Real-time PCR analysis of mRNAs encoding NOX isoforms in neonatal adrenal medullae from P5 aged rats. Results are expressed as fold change compared with 18S mRNA. Data presented are mean ± SEM from three individual experiments performed in triplicate. $*p < 0.05$; $**p < 0.01$. ***B***, Localization of NOX2 and NOX4 in adrenal chromaffin cells from P5 aged rats. Left, NOX2-like immunoreactivity (green) is seen in cytoplasm of chromaffin cells; nucleus is stained with 4′,6′-diamidino-2-phenylindole (blue). Right, NOX4-like immunoreactivity is seen in nucleus (red); tyrosine hydroxylase-like immunoreactivity as a marker of chromaffin cells (green). Scale bars, 15 μm. ***C***, Effect of IH on NOX2 and NOX4 mRNA expression in neonatal adrenal medullae. Results are expressed as fold change with respect to normoxic controls. Data presented are mean ± SEM from three individual experiments performed in triplicate. $**p < 0.01$. ***D***, Effect of IH on NOX enzyme activity. Adrenal medullae were harvested from rat pups exposed to IH from ages P0–P5 or normoxia and NOX enzyme activity was determined as described in Materials and Methods. Note the increased NOX activity in IH-treated adrenal medullae. Data presented are mean ± SEM from six individual experiments performed in triplicate. $**p < 0.001$ compared with controls.

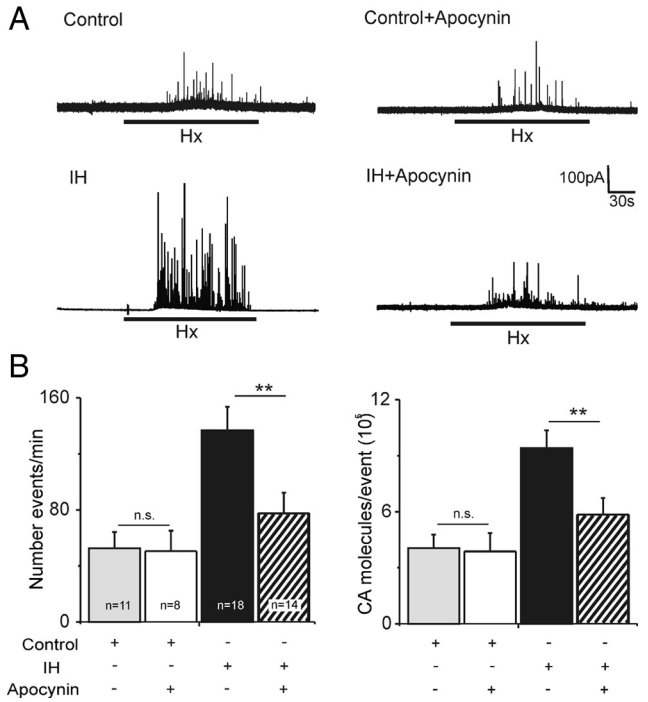

Figure 2. NOX inhibitor prevents the effects of IH on neonatal chromaffin cell secretory response to hypoxia. ***A***, Examples of hypoxia-evoked catecholamine secretion from chromaffin cells from P5 rats reared under normoxia (Control) or normoxia treated with apocynin (10 mg/kg, i.p., from P0–P5), an inhibitor of NOX (top) and IH or IH-treated with apocynin (bottom). The horizontal black bars represent the duration of hypoxia (HX; PO_2 of ~30 mmHg) challenge. ***B***, Average data showing the number of secretory events per minute (left) and average CA molecules released per event (right). *n* indicates number of cells obtained from three different litters in each group. Results presented are mean ± SEM. $**p < 0.001$ compared with untreated controls. n.s., Not significant; $p > 0.05$ compared with corresponding controls.

tal adrenal chromaffin cells reported that activation of T-type Ca^{2+} channels (low voltage-gated Ca^{2+} channels) is critical for mediating catecholamine secretion by hypoxia (Levitsky and López-Barneo, 2009). Additionally, exposing adult chromaffin cells to 12–18 h of hypoxia can upregulate T-type Ca^{2+} channels that facilitate exocytosis (Carabelli et al., 2007). Whether T-type Ca^{2+} channels contribute to the effects of IH on catecholamine secretion from neonatal chromaffin cells has not been examined. Although mobilization of intracellular Ca^{2+} stores plays little or no role in hypoxia-induced $[Ca^{2+}]_i$ changes in neonatal rat chromaffin cells (Takeuchi et al., 2001), our recent study suggests that IH mobilizes Ca^{2+} stores in neonatal adrenal chromaffin cells (Souvannakitti et al., 2009). However, the source(s) of intracellular Ca^{2+} stores and the mechanism by which IH mobilizes Ca^{2+} stores has not been explored. Ryanodine receptors (RyRs) are one of the major regulators of mobilization of intracellular Ca^{2+} stores (Simpson et al., 1995; Alonso et al., 1999), and ROS are potent activators of RyRs (Murayama et al., 1999; Zissimopoulos and Lai, 2006; Bull et al., 2008; Huddleston et al., 2008; Belevych et al., 2009). Therefore, in the present study, we examined the impact of neonatal IH on T-type Ca^{2+} channels and RyRs expression in adrenal chromaffin cells and determined their roles in neurotransmitter release.

Materials and Methods

Experimental protocols were approved by the Institutional Animal Care and Use Committee of the University of Chicago. All experiments were performed on neonatal Sprague Dawley rat pups of either sex ages from P0 to P5.

Exposure to intermittent hypoxia. Rat pups (P0) along with their mothers were exposed to IH (15 s at 10% O_2, followed by 5 min at 21% O_2; 8 h/d) for 5 d (P0–P5; between 9:00 A.M. and 5:00 P.M.) as described previously (Pawar et al., 2008; Souvannakitti et al., 2009). Briefly, rat pups along with their mothers were housed in feeding cages and placed in a chamber designed for exposure to IH. The animals were unrestrained, freely mobile, and fed *ad libitum*. The chamber was flushed with alternating cycles of nitrogen gas and room air. Inspired O_2 levels reached a nadir of 10% O_2 during hypoxia. O_2 and CO_2 levels in the chamber were continuously monitored, and ambient CO_2 levels were maintained between 0.2 and 0.5%. Control experiments were performed on age-matched rat pups exposed to normoxia. In the protocols involving antioxidant treatment, rat pups were given manganese (III) tetrakis (1-methyl-4-pyridyl) porphyrin pentachloride (MnTMPyP) (5 $mg \cdot kg^{-1} \cdot d^{-1}$, i.p.; Alexis Biochemicals), a membrane-permeable superoxide dismutase mimetic or apocynin (10 $mg \cdot kg^{-1} \cdot d^{-1}$, i.p.), an inhibitor of NOX, every day before placing rats in the IH chamber. Rat pups treated with vehicle (saline) served as controls. Acute experiments were performed on anesthetized pups (1.2 g/kg urethane, i.p.) 6–10 h after either IH or normoxia.

Preparation of chromaffin cells and cell culture. Adrenal glands were harvested from IH and control rat pups anesthetized with urethane (1.2 g/kg, i.p.). The adrenal cortex was removed, and the medullary chromaffin cells were enzymatically dissociated using a mixture of collagenase P (2 mg/ml; Roche), DNase (25 μg/ml; Sigma), and BSA (3 mg/ml; Sigma) at 37°C for 30 min, followed by a 15 min digestion in 0.03% trypsin/EDTA (Invitrogen) and DNase (50 μg/ml;Sigma). Cells were plated on collagen (type VII; Sigma)-coated coverslip and maintained at 37°C in a 5% CO_2 incubator for 12–24 h. The growth medium consisted of F-12 K

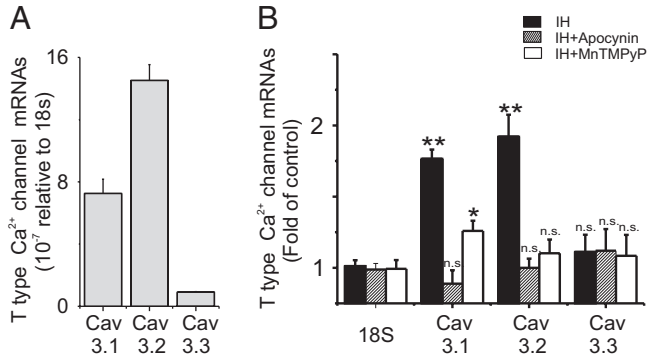

Figure 3. Effect of IH on T-type Ca^{2+} channel mRNA levels in neonatal adrenal chromaffin cells. ***A***, Real-time PCR analysis of mRNAs encoding Cav3.1, Cav3.2, and Cav3.3 T-type Ca^{2+} channels in neonatal adrenal medullae from P5 control rats. Results are expressed as fold change compared with 18S mRNA. Data presented are mean ± SEM from three individual experiments performed in triplicate. The mRNA levels of Cav3.1 and Cav3.2 were relatively higher than Cav3.3. ***B***, Effect of IH on Cav3.1, Cav3.2, and Cav3.3 mRNA levels in neonatal adrenal medullae. Results are expressed as fold change compared with normoxic controls. IH-upregulated Cav3.1 and Cav3.2 and apocynin (NOX inhibitor) or MnTMPyP (O_2^- scavenger) prevented this effect. Data presented are mean ± SEM from three individual experiments performed in triplicate. $^{**}p < 0.001$ compared with controls. n.s., Not significant; $p > 0.05$.

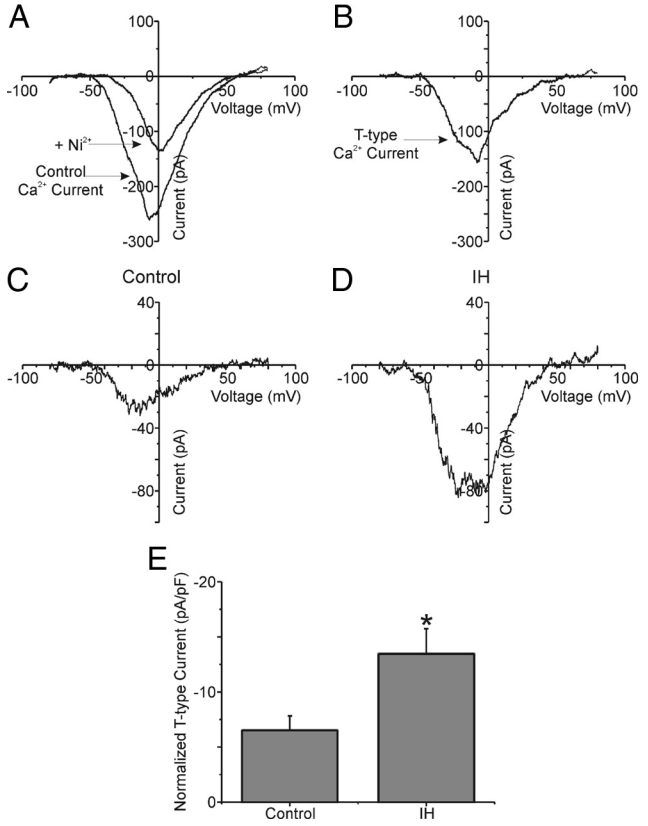

Figure 4. IH treatment upregulates T-type Ca^{2+} current in neonatal chromaffin cells. For these experiments, voltage ramps from −80 to +80 mV, lasting 150 ms, were used to stimulate chromaffin cells. Extracellular TEA-based and intracellular Cs-based solutions were used to suppress voltage-gated Na and K channel currents. ***A*** plots Ca^{2+} currents obtained in the absence (larger current) and presence (smaller current) of 100 μM $NiCl_2$, a relatively selective blocker of T-type Ca^{2+} current. ***B*** plots the isolated T-type Ca^{2+} channel current obtained after subtracting the smaller current from the larger current in ***A***. This method was used for all the data presented in this manuscript. ***C***, ***D***, Plots represent T-type Ca^{2+} currents obtained from normoxia- and IH-treated chromaffin cells. Both cells were 6 pF and were stimulated by identical voltage ramps. ***E***, Plots the average of the peak T-type Ca^{2+} currents obtained from normoxia ($n = 5$) and IH-treated cells ($n = 8$). IH treatment resulted in a T-type Ca^{2+} current that was significantly larger than control ($p < 0.05$).

medium (Invitrogen) supplemented with 10% horse serum, 5% fetal bovine serum, and 1% penicillin/streptomycin/glutamine mixture (Invitrogen).

Measurements of catecholamine secretion by amperometry. Catecholamine secretion from chromaffin cells was monitored by amperometry using carbon fiber electrodes as described previously (Souvannakitti et al., 2009). The electrode was held at +700 mV versus a ground electrode using an NPI VA-10 amplifier to oxidize catecholamine transmitter. The amperometric signal was low-pass filtered at 2 kHz (eight-pole Bessel; Warner Instruments) and sampled into a computer at 10 kHz using a 16-bit analog-to-digital converter (National Instruments). Records with root-mean-square noise >2 pA were not analyzed. Amperometric spike features, quantal size, and kinetic parameters were analyzed using a series of macros written in Igor Pro (WaveMetrics) kindly supplied by Dr. Eugene Mosharov (Columbia University, New York, NY). The detection threshold for an event was set at four to five times the root-mean-square noise and the spikes were automatically detected. The area under individual amperometric spikes is equal to the charge (picocoulombs) per release event, referred to as *Q*. The number of oxidized neurotransmitter molecules (*N*) was calculated using the Faraday equation, $N = Q/ne$, with $n = 2$ electrons per oxidized molecule of transmitter, and *e* is the elemental charge (1.603×10^{-19} C). Because the number of events varied considerably from cell to cell, the data from each cell was averaged to provide a single number for the overall statistic using the technique described by Colliver et al. (2000).

Amperometric recording solutions and stimulation protocols. Amperometric recordings were made from adherent cells that were under constant perfusion (flow rate of ~1.0 ml/min; chamber volume, ~80 μl). All experiments were performed at ambient temperature (23 ± 2°C), and the solutions had the following composition (in mM): 1.26 $CaCl_2$, 0.49 $MgCl_2$–6 H_2O, 0.4 $MgSO_4$–$7H_2O$, 5.33 KCl, 0.441 KH_2PO_4, 137.93 NaCl, 0.34 Na_2HPO_4–$7H_2O$, 5.56 dextrose, and 20 HEPES, pH 7.35 (300 mOsm). Normoxic solutions were equilibrated with room air (PO_2 of ~146 mmHg). For challenging with hypoxia, solutions were degassed and equilibrated with appropriate gas mixtures that resulted in final medium PO_2 of 30 mmHg as measured by blood gas analyzer. Ca^{2+}-free solutions contained 0.5 mM EGTA.

Measurements of T-type Ca^{2+} current by electrophysiology. Chromaffin cells were voltage clamped in the whole-cell configuration of the patch-clamp technique using an Axopatch 1D amplifier (Molecular Devices) at a holding potential of −80 mV. Current–voltage information was generated by voltage ramps of 150 ms duration from −80 to +80 mV. Leak currents were generated by voltage ramps from −80 to −60 mV that were scaled appropriately. The data were filtered at 2 kHz and then digitized at 100 μs per point. Voltage protocols and data analysis were performed in WinWCP (from The University of Strathclyde, Strathclyde, Scotland, UK). Additional analysis was performed using Origin. Statistical significance was determined using an independent Student's *t* test. Electrodes were pulled from microhematocrit capillary tubes. After fire polishing, final electrode resistances when filled with the CsCl-based patch pipette solution (see below) were ~2 MΩ. Electrodes were filled with the following (in mM): 100 CsCl, 5 $MgCl_2$, 40 HEPES, 10 EGTA, and 2 ATP, pH 7.3 (adjusted by CsOH, ≈295 mOsm). Recordings were made in a tetraethylammonium (TEA)-based extracellular solution contained the following (in mM): 140 TEA-Cl, 10 glucose, 10 HEPES, and 10 $CaCl_2$, pH 7.3 (adjusted by TEA-OH). $NiCl_2$ was prepared as a 100 mM stock solution in distilled water and then added directly to the TEA recording solution to a final concentration of 100 μM.

Measurements of $[Ca^{2+}]_i$. $[Ca^{2+}]_i$ was monitored in chromaffin cells as described previously (Souvannakitti et al., 2009). Briefly, chromaffin cells were incubated in HBSS with 2 μM fura-2 AM and 1 mg/ml albumin for 30 min and washed in a fura-2-free solution for 30 min at 37°C. The coverslip was transferred to an experimental chamber for recording. Background fluorescence at 340 and 380 nm wavelengths were obtained using an area of the coverslip devoid of cells. Data were continuously collected throughout the experiment. On each coverslip, four to eight chromaffin cells were selected and individually imaged. Image pairs (one at 340 and the other at 380 nm) were obtained every 2 s by averaging 16

frames at each wavelength. Background fluorescence was subtracted from the individual wavelengths, and the 340 nm image was divided by the 380 nm image to provide a ratiometric image. Ratios were converted to free $[Ca^{2+}]_i$ by comparing data to fura-2 calibration curves made *in vitro* by adding fura-2 (50 μM free acid) to solutions that contained known concentrations of calcium (0–2000 nM). The recording chamber was continually superfused with solution from gravity-fed reservoirs.

Measurements of NADPH oxidase enzyme activity. NADPH oxidase activity was determined by monitoring O_2^--dependent reduction of ferric cytochrome *c* at 550 nm as described previously (Mayo and Curnutte, 1990). Briefly, freshly harvested adrenal medullae were placed in PBS, 0.9 mM $CaCl_2$, 0.5 mM $MgCl_2$, and 7.5 mM glucose, pH 7.4. The reaction was initiated by addition of cytochrome *c* (75 μM) to the reaction medium. Increase in the absorbance was monitored at 550 nm for 5 min. The amount of reduced cytochrome *c* formed during the reaction was determined using the molar extinction coefficient of 20.5 μmol/cm^{-2}. Reduction of cytochrome *c* was prevented by inhibitors of NADPH oxidase (3 μM diphenyl iodinium and 500 μM apocynin). The enzyme activity was expressed as nanomoles per minute per milligram of protein.

Real-time reverse transcription-PCR assay for determining mRNA expression. Real-time reverse transcription (RT)-PCR was performed using a MiniOpticon system (Bio-Rad) with SYBR GreenER two-step quantitative RT-PCR kit (catalog #11764-100; Invitrogen) as described previously (Peng et al., 2009). Briefly, RNA was extracted from adrenal medullae using TRIZOL and was reverse transcribed using superscript III reverse transcriptase. Primer sequences for real time RT-PCR amplification were as follows: 18S forward (fw), GTAACCCGTTGAACCCCATT; 18S reverse (rev), CCATCCAATCGGTAGTAGCG (size, 151; GenBank accession number X_01117); NOX1 fw, CACTGTGGCTTTGGTTCTA; NOX1 rev, TGAGGACTCCTGCAACTCCT (size, 240; GenBank accession number NM_053683); NOX2 fw, GTGGAGTGGTGTGAATGC; NOX2 rev, TTTGGTGGAGGATGTGATGA (size, 219; GenBank accession number NM_023965); NOX3 fw, GACCCAACTGGAATGAGGAA; NOX3 rev, AATGAACGACCCTAGGATCT (size, 150; GenBank accession number NM_001004216); NOX4 fw, CGGGGTGGCTTGTTGAAGTAT; NOX4 rev, CGGGGTGGCTTGTTGAAGTAT (size, 205; GenBank accession number NM_053524); Cav3.1 fw, 5′CTTTGACCTGCCTGACACTCTG; Cav3.1 rev, GCCATTACAGTCTTGGTGCTCA (size, 185; GenBank accession number AF290212); Cav3.2 fw, ACTTGGCCATCGTCCTCCTA; Cav3.2 rev, ATGGTGGGATTGATGGGCAG (size, 101; GenBank accession number AF290213); Cav3.3 fw, GACCCCA GAG CAGTGAGGAT; Cav3.3 rev, TACTTG CTGTCCACGA TGCC (size, 155; GenBank accession number AF 290214); RyR1 fw, AAGAAGGAGGAAGCTGGAGGTG; RyR1 rev, TGGCGGAGAGTCTGA AACCTTA (size, 212; GenBank accession number XM341818); RyR2 fw, CAACCAGCAC CTGCTGAG AA; RyR2 rev, ATAGCAAGCTGCATAGCCCG (size, 178; GenBank accession number EU346200); RyR3 fw, AATGACTCTCAGCACAGGAG GG; and RyR3 rev, AGAAGGCTGTGGACTTGGTGTC (size, 232; GenBank accession number XM342491). Relative mRNA level was calculated using the comparative threshold (CT) method using the formula 2 − CT, where CT is the difference between the threshold cycle of the given target cDNA between normoxia and IH. The CT value was taken as a fractional cycle number at which the emitted fluorescence of the sample passes a fixed threshold above the baseline. Values were compared with an internal standard gene 18S. Purity and specificity of all products were confirmed by omitting the template and by performing a standard melting curve analysis.

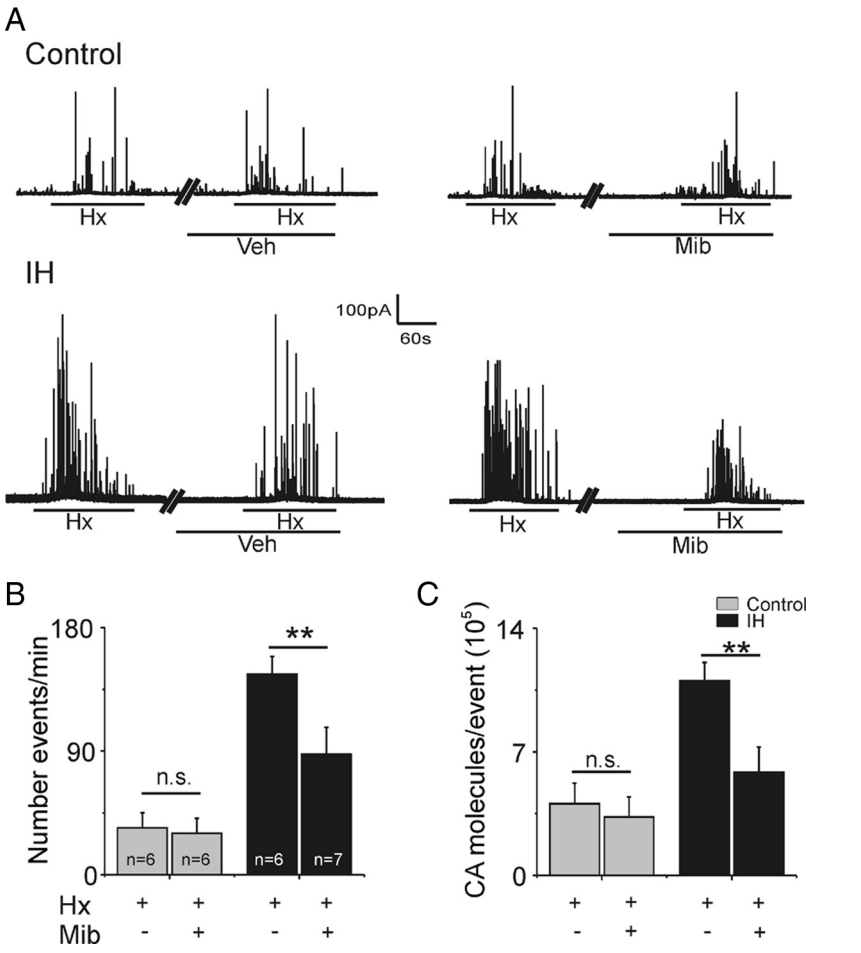

Figure 5. Effect of T-type Ca^{2+} channel inhibitor on hypoxia-evoked catecholamine secretion in IH-treated neonatal adrenal chromaffin cells. ***A***, Examples illustrating the effects of mibefradil (Mib; 10 μM), an inhibitor of Cav3.1 and Cav3.2 on hypoxia-evoked catecholamine secretion from adrenal chromaffin cells from normoxia-treated (control; top) or IH-treated (bottom) rats. Hx, Hypoxia (PO_2 of ~30 mmHg); Mib, mibefradil; Veh, vehicle. Horizontal black bars indicate the duration of challenges. ***B***, Average data showing the number of secretory events per minute (left). ***C***, Average CA molecules released per event (right). *n* indicates number of cells obtained from three different litters in each group. Results presented are mean ± SEM. $^{**}p < 0.001$. n.s., not significant; $p > 0.05$ compared with untreated controls.

Western blot assays. Immunoblot assays were performed as described previously (Yuan et al., 2008). Briefly, rat adrenal medullae were homogenized in 3-(*N*-morpholino)-propanesulfonic acid/Tris/sucrose buffer, and endoplasmic reticulum (ER) vesicles were isolated by differential centrifugation (Marengo et al., 1996). ER vesicles were fractionated by 4–15% SDS-PAGE under nonreducing conditions and transferred to a polyvinylpyrrolidone difluoride membrane (Immobilon-P; Millipore Corporation). The membrane was blocked with Tris-buffered saline-Triton X-100 (TBS-T) containing 5% nonfat milk at 4°C overnight. Membranes were incubated with anti-RyR2 and anti-RyR3 antibody (1:500; Millipore Corporation) in TBS-T containing 3% nonfat milk. Membranes were treated with goat anti-rabbit secondary antibody conjugated with horseradish peroxidase (1:2000; Santa Cruz Biotechnology) in TBS-T containing 3% nonfat milk. Immune complexes on the membrane were visualized using a chemiluminescence (ECL) detection system (GE Healthcare). The membranes were exposed to Kodak XAR films.

Measurements of S-glutathionylation of RyR isoforms. Membranes were probed with anti-glutathione (GSH) antibody (1:1000; Invitrogen). After immunodetection, membranes were stripped and reprobed with either

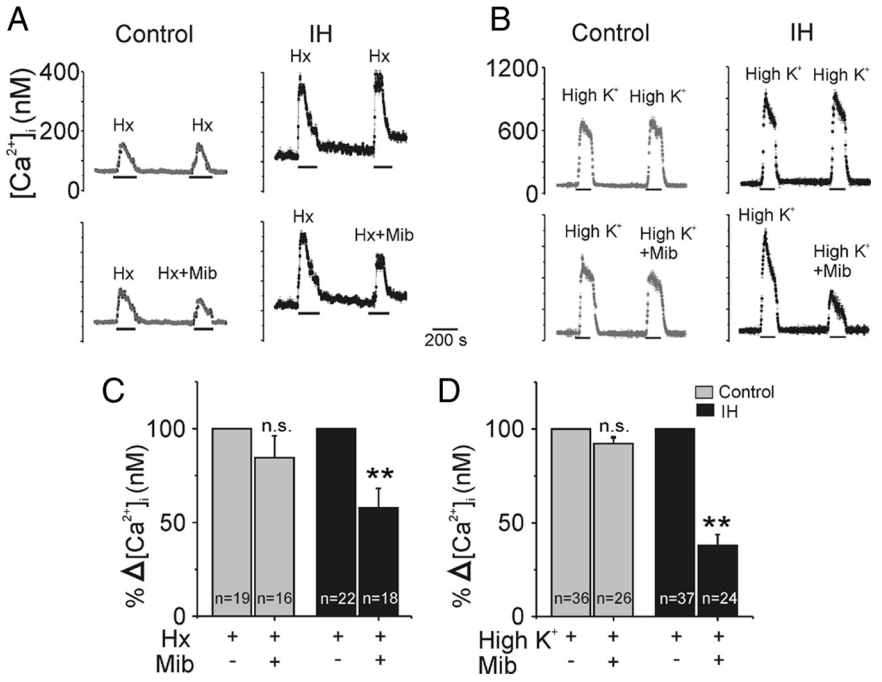

Figure 6. Effect of T-type Ca^{2+} channel inhibitor on hypoxia and high K^+-evoked $[Ca^{2+}]_i$ changes in neonatal rat chromaffin cells. ***A***, ***B***, Examples illustrating $[Ca^{2+}]_i$ responses to acute hypoxia (Hx; PO_2 of ~30 mmHg) or high K^+ (40 mM) with and without mibefradil (Mib; 10 μM) determined every 2 s in individual chromaffin cells from rats exposed to either normoxia (control) or IH from ages P0–P5. Mib, 10 μM mibefradil. Horizontal black bars represent the duration of the hypoxia or K^+ challenge. ***C***, ***D***, Average data of hypoxia (***C***) and K^+-induced $[Ca^{2+}]_i$ changes (***D***) with and without mibefradil. Results represent change (Δ) in $[Ca^{2+}]_i$ (i.e., stimulus-basal) presented as percentage change from control (i.e., without mibefradil). Data are mean ± SEM. *n* indicates number of cells obtained from three different litters in each group. $^{**}p < 0.001$.

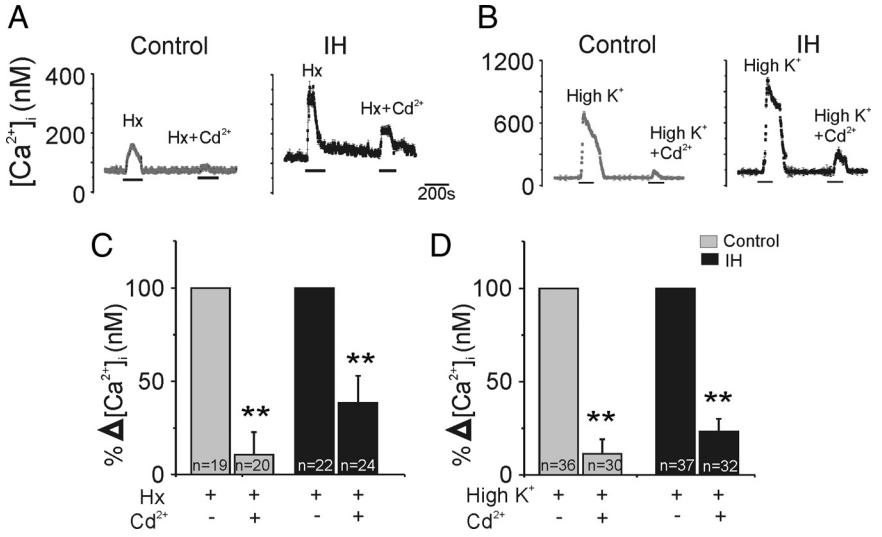

Figure 7. Effect of Cd^{2+} on hypoxia and high K^+-evoked $[Ca^{2+}]_i$ changes in neonatal rat chromaffin cells. ***A***, ***B***, Examples illustrating $[Ca^{2+}]_i$ responses to hypoxia (Hx; PO_2 of ~30 mmHg) or high K^+ (40 mM) with and without Cd^{2+} (300 μM) determined every 2 s in individual chromaffin cells from rats exposed to normoxia (control) or IH. Horizontal black bars represent the duration of the hypoxia and K^+ challenges. ***C***, ***D***, Average data of $[Ca^{2+}]_i$ changes in response to hypoxia and K^+ with and without Cd^{2+} from control and IH-treated cells. Results presented are changes (Δ) in $[Ca^{2+}]_i$ (i.e., stimulus-basal) normalized as percentage change from control (i.e., without Cd^{2+}). Data are mean ± SEM. *n* indicates number of cells obtained from three different litters in each group. $^{**}p < 0.001$ compared with controls.

anti-RyR2 (1:500; Millipore Corporation) or anti-RyR3 (1:500; Millipore Corporation) antibodies. Immune complexes on the membrane were visualized using an ECL detection system (GE Healthcare). The membranes were exposed to Kodak XAR films. S-Glutathionylation levels were expressed as the ratio of anti-GSH to anti-RyR band densities (Sánchez et al., 2005).

Data analysis. Statistical analyses between experimental groups are presented as means ± SEM, and Student's *t* test was used for statistical comparisons between two groups. $p < 0.05$ were considered significant.

Results

NOX activation is required for IH-evoked facilitation of catecholamine secretion by hypoxia

Several NOX isoforms have been identified (for references, see Bedard and Krause, 2007). To determine which of the NOX isoforms are expressed in the neonatal rat adrenal chromaffin cells, mRNA levels of NOX1–NOX4 were examined by quantitative real-time PCR. Neonatal adrenal medullae expressed high levels of NOX2 and NOX4 relative to NOX1 and NOX 3 mRNAs (Fig. 1*A*). Immunocytochemical analysis showed that NOX2-like immunoreactive product was primarily localized to the cytoplasm, whereas the localization of NOX4-like immunoreactivity was confined to the nucleus (Fig. 1*B*). After 5 d of IH treatment, NOX2 and NOX4 mRNAs as well as the NOX enzyme activity were significantly elevated compared with control adrenal medullae ($p < 0.01$ to $p < 0.001$) (Fig. 1*C*,*D*).

To assess the functional significance of NOX activation, rat pups were treated with apocynin, an inhibitor of NOX, or the vehicle for 5 d before subjecting them to IH or to normoxia (controls). Hypoxia-evoked catecholamine secretion was monitored from chromaffin cells harvested from both groups of pups. Examples illustrating the hypoxia-evoked catecholamine secretion and the average data are summarized in Figure 2. Apocynin treatment completely prevented the augmented secretory responses to hypoxia in IH-treated cells, whereas it had no effect in cells from control rat pups reared under normoxia.

IH upregulates T-type Ca^{2+} channel mRNAs via NOX/ROS signaling

Neonatal adrenal medullae expressed higher levels of Cav3.1 and Cav3.2 mRNAs compared with Cav3.3 (Fig. 3*A*). After IH treatment, Cav3.1 and Cav3.2 mRNAs were upregulated, whereas $Ca_v3.3$ mRNA expression was unaltered compared with control adrenal medullae (Fig. 3*B*). Systemic administration of apocynin, an inhibitor of NOX, or MnTMPyP, an O_2^- scavenger, prevented or markedly attenuated IH-induced upregulation of Cav3.1 and Cav3.2 mRNAs in neonatal adrenal medullae (Fig. 3*B*).

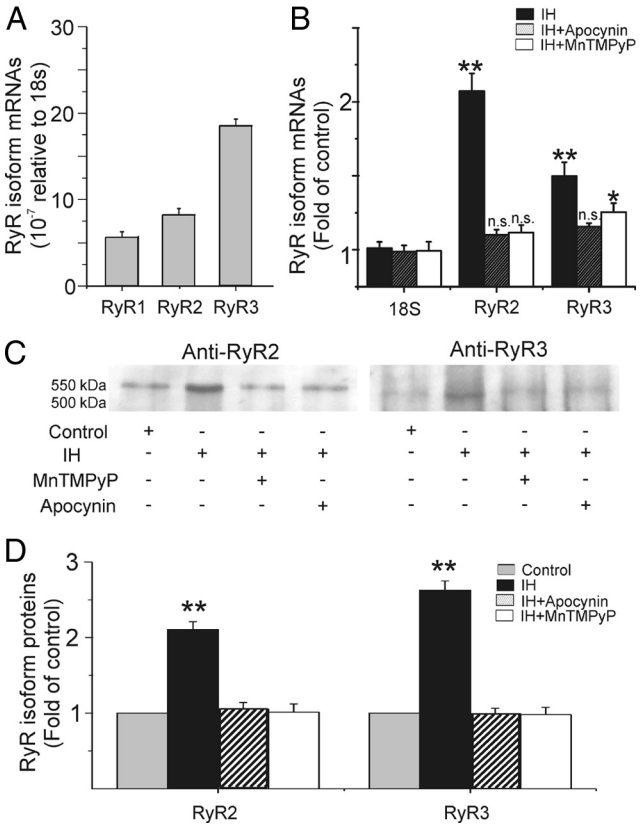

Figure 8. IH upregulates RyR isoforms in neonatal rat adrenal medullae. ***A***, Real-time PCR analysis of mRNAs encoding RyR1–RyR3 in adrenal medullae from P5 control rats. Results are expressed as fold change compared with 18S mRNA. Data represent mean ± SEM from three individual experiments performed in triplicate. ***B***, Effect of apocynin and MnTMPyP on IH-evoked changes in RyR1–RyR3 mRNA expressions in adrenal medullae. The data presented are fold changes from control adrenal medullae (i.e., control = 1). IH upregulated RyR2 and RyR3 mRNAs, and these effects were abolished by apocynin or MnTMPyP. Data presented are mean ± SEM from three individual experiments performed in triplicate. $^{**}p < 0.001$. n.s., Not significant; $p > 0.05$ compared with controls. ***C***, ***D***, Representative Western blot (***C***) and densitometric analysis of changes (***D***) of RyR2 and RyR3 protein expressions in control, IH-treated, and IH + apocynin-treated or IH + MnTMPyP-treated adrenal medullae. ***D***, Densitometric analysis of changes in RyR2 and RyR3 proteins in adrenal medullae from control, IH-treated, and IH + apocynin-treated or IH + MnTMPyP-treated rat. Data presented are mean ± SEM from three individual experiments performed in triplicate. $^{**}p < 0.001$ compared with controls.

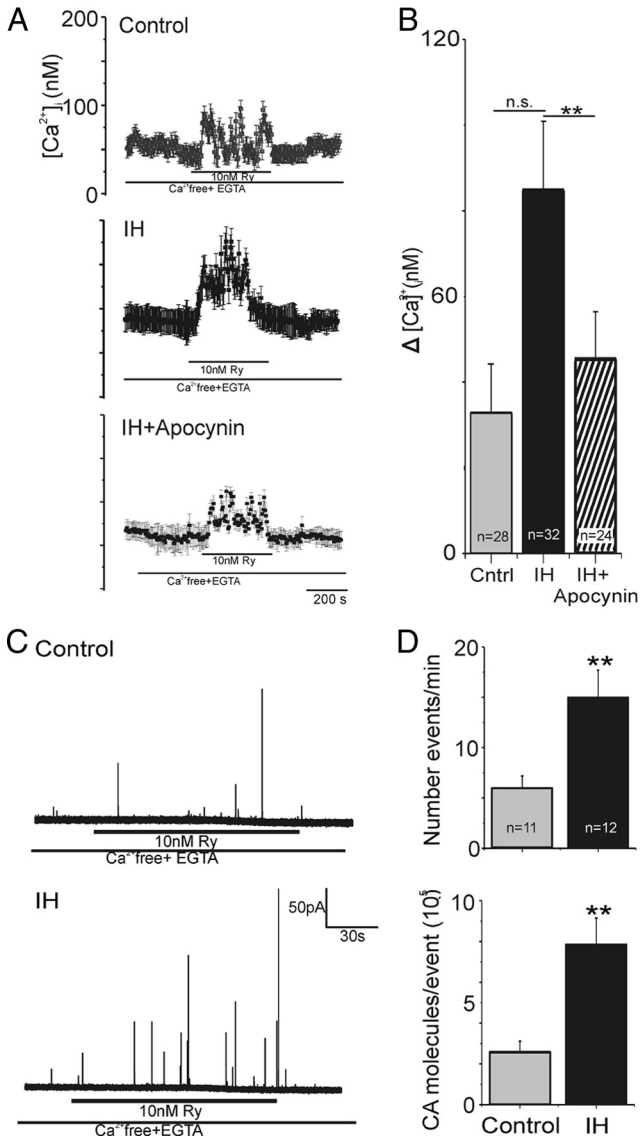

Figure 9. Effects of IH on ryanodine receptor agonist-evoked changes in $[Ca^{2+}]_i$ and catecholamine secretion from neonatal chromaffin cells. ***A***, Examples illustrating $[Ca^{2+}]_i$ responses to 10 nM ryanodine, an RyR agonist analyzed every 2 s in individual chromaffin cells from P5 control rats or IH- or apocynin-treated IH rats (IH+Apocynin). Experiments were performed in Ca^{2+}-free + EGTA (0.5 mM) containing medium. Horizontal black bars represent the duration of the ryanodine (Ry) challenge. ***B***, Average data of ryanodine-evoked changes in $[Ca^{2+}]_i$ presented as change (Δ) (stimulus-baseline) in chromaffin cells from control, IH-treated, and IH rats treated with apocynin (IH+Apocynin). Data represent mean ± SEM. *n* represents number of cells obtained from three different litters in each group. $^{**}p < 0.001$. n.s., Not significant; $p > 0.05$ compared with controls. ***C***, Examples illustrating the effects of ryanodine-evoked catecholamine secretion from chromaffin cells derived from rats treated with either normoxia (control) or IH from ages P0 –P5. Horizontal black bars represent the duration of the ryanodine (10 nM Ry) challenge. ***D***, Average data of the effects of ryanodine on catecholamine secretion showing the number of secretory events per minute (top) and the average catecholamine molecules released per event (bottom). Data represent mean ± SEM. *n* represents number of cells from three different litters in each group. $^{**}p < 0.001$ compared with controls.

IH increases T-type Ca^{2+} current in adrenal chromaffin cells

Unlike adult cells, neonatal chromaffin cells express T-type Ca^{2+} channels (Levitsky and López-Barneo, 2009). Nevertheless, neonatal chromaffin cells from IH-treated rats exhibited significantly larger T-type Ca^{2+} currents than did cells from control animals. $NiCl_2$, at an appropriate concentration, is a relatively selective blocker of T-type Ca^{2+} channels. Voltage ramps were performed before and after application of 100 μM Ni^{2+} to isolate the T-type component. Ionic conditions were chosen that isolated voltage-gated Ca^{2+} current by suppressing voltage-gated Na^+ and K^+ channels (see Materials and Methods). Figure 4, *A* and *B*, illustrates the method used for isolating T-type Ca^{2+} current. The larger current in *A* shows a leak-subtracted current obtained in response to a voltage ramp from −80 to +80 mV (lasting 150 ms). The smaller of the currents was obtained using an identical voltage protocol but in the presence of 100 μM Ni^{2+}. In particular, note the blockade of Ca^{2+} currents at negative voltages. The difference between the two current traces represents the T-type current and is shown in Figure 4*B*. Figure 4, *C* and *D*, shows typical T-type Ca^{2+} currents, obtained after Ni^{2+} subtraction, from control and IH-treated chromaffin cells, elicited by voltage ramps. Because the data were obtained from cells that were identical in size (6 pF), the currents can be directly compared. Figure 4*E* shows averaged data comparing the peak amplitude of T-type Ca^{2+} current from control and IH-treated cells. The T-type currents from IH-treated cells were significantly larger than control cells ($p < 0.05$).

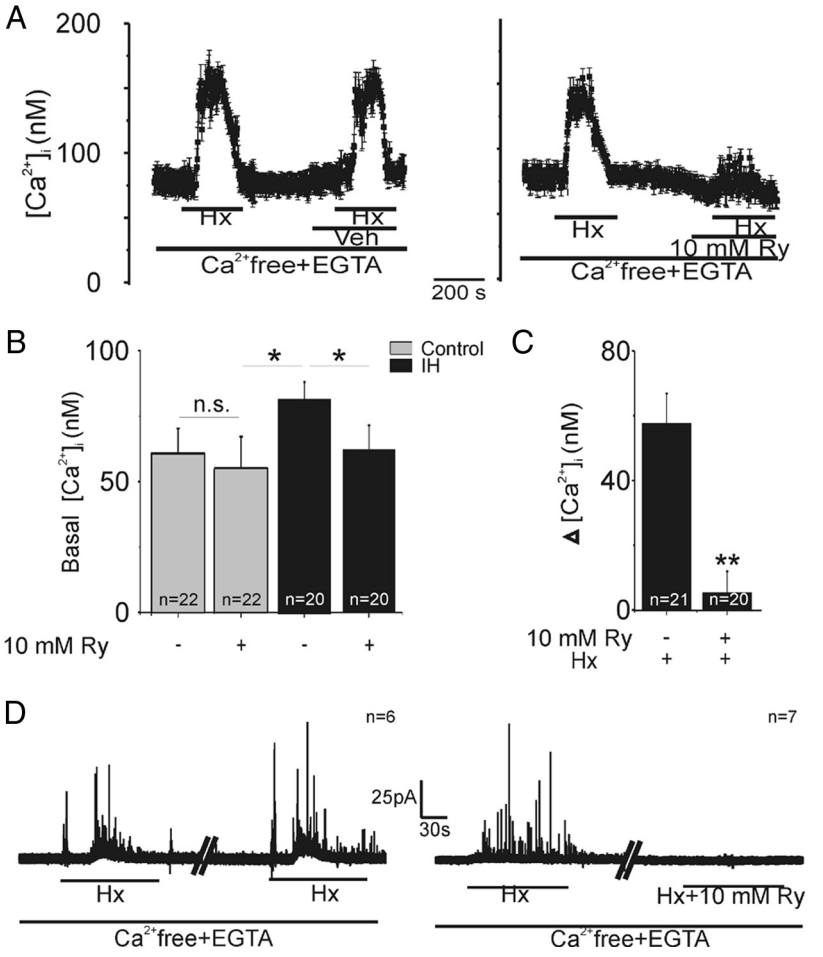

Figure 10. Effect of RyR blockade on hypoxia-evoked $[Ca^{2+}]_i$ elevations and CA secretion with Ca^{2+}-free medium in IH-treated neonatal chromaffin cells. ***A***, Representative examples of $[Ca^{2+}]_i$ response to hypoxia (Hx) in IH-treated chromaffin cells either in the presence of vehicle (Veh) or blockade of RyR with 10 mM ryanodine (Ry) in Ca^{2+}-free medium plus 0.5 mM EGTA. Horizontal black bars represent the duration of hypoxic challenge. Note the decrease in basal $[Ca^{2+}]_i$ as well as attenuated $[Ca^{2+}]_i$ response to hypoxia in the presence of 10 mM Ry. ***B***, ***C***, Average data showing the effect of 10 mM ryanodine (Ry) on basal $[Ca^{2+}]_i$ in control and IH-treated cells (***B***) and $[Ca^{2+}]_i$ response to hypoxia in IH-treated cells (***C***). Experiments were performed in Ca^{2+}-free medium plus 0.5 mM EGTA. Data presented are mean ± SEM. *n* represents number of cells obtained from three different litters in each group. $*p < 0.01$. n.s., Not significant; $p > 0.05$ compared with controls. ***D***, Examples illustrating hypoxia-evoked catecholamine secretion in Ca^{2+}-free medium plus 0.5 mM EGTA from IH-treated chromaffin cells with and without 10 mM ryanodine. Note the absence of hypoxia-induced catecholamine secretion in the presence of 10 mM ryanodine.

T-type Ca^{2+} channels contribute to IH-evoked facilitation of catecholamine secretion

To determine the functional significance of T-type Ca^{2+} channels, hypoxia-evoked catecholamine secretion was monitored in control and IH-treated chromaffin cells in the presence or absence of 10 μM mibefradil, a T-type Ca^{2+} channel blocker (Randall and Tsien, 1997; Martin et al., 2000; Kuri et al., 2009). Examples of secretory responses and the average data are shown in Figure 5*A*. Mibefradil had no significant effect on hypoxia-evoked catecholamine secretion in control cells, whereas it significantly attenuated the secretory response in IH-treated cells. The attenuated catecholamine secretion by mibefradil was attributable to a significant reduction in the number secretory events as well as amount of catecholamine secreted per release event (Fig. 5*B*,*C*).

We examined the contribution of T-type Ca^{2+} channels to Ca^{2+} influx elicited by hypoxia in IH-treated and control chromaffin cells. Basal Ca^{2+} (control, 66.2 ± 5 nM vs IH, 110.3 ± 10.5 nM; $p < 0.01$) and hypoxia-evoked elevations in $[Ca^{2+}]_i$ were significantly higher in IH compared with control cells (Fig. 6*A*), a finding consistent with our previous study (Souvannakitti et al., 2009). Mibefradil attenuated the hypoxia-evoked elevation of $[Ca^{2+}]_i$ in IH-treated cells more than in control cells (Fig. 6*A*). On average, mibefradil inhibited hypoxia-evoked $[Ca^{2+}]_i$ by ~15% in control cells as opposed to ~43% inhibition in IH-treated cells ($p < 0.01$) (Fig. 6*C*). However, mibefradil had no significant effect on baseline $[Ca^{2+}]_i$ ($p > 0.05$). Similar results were also obtained by stimulating chromaffin cells with high K^+ (Fig. 6*B*,*D*). In striking contrast, 300 μM Cd^{2+}, a blocker of all voltage-gated Ca^{2+} channels but with a preference for high-threshold Ca^{2+} channels, inhibited the hypoxia-evoked elevation of $[Ca^{2+}]_i$ more in control compared with IH-treated cells (Cd^{2+}-evoked inhibition: control, ~90% vs IH-treated cells, ~60% inhibition; $p < 0.01$) (Fig. 7*A*,*C*). Similar results for Cd^{2+} were also observed when cells were stimulated with high K^+ (Fig. 7*B*,*D*).

IH upregulates ryanodine receptor mRNAs via NOX/ROS signaling

Our previous study suggested that IH-treated cells mobilize Ca^{2+} from intracellular stores more efficiently than in control chromaffin cells (Souvannakitti et al., 2009). RyR1–RyR3 are the major regulators of intracellular Ca^{2+} mobilization (Alonso et al., 1999). As shown in Figure 8*A*, neonatal adrenal medullae expressed mRNAs encoding all three isoforms of RyRs, including RyR1–RyR3. However, mRNA levels of RyR3 were relatively higher than RyR1 and RyR2 mRNAs. After IH treatment, RyR2 and RyR3 mRNAs as well as the levels of corresponding proteins were upregulated (Fig. 8*B–D*), whereas the RyR1 mRNA was unaffected (Fig. 8*B*). Systemic administration of apocynin or MnTMPyP prevented the upregulation of RyR2 and RyR3 mRNA and the protein expression in IH-treated adrenal medullae (Fig. 8*B–D*).

To assess the functional significance of RyR2 and RyR3 upregulation, $[Ca^{2+}]_i$ and catecholamine secretions were monitored in control and IH-treated chromaffin cells in a Ca^{2+}-free medium in response to low concentrations of ryanodine (10 nM), which serves as an agonist of RyRs. Ryanodine produced a greater elevation of $[Ca^{2+}]_i$ and more pronounced catecholamine secretion in IH-treated compared with control cells (Fig. 9).

RyRs contribute to augmented $[Ca^{2+}]_i$ and secretory responses to hypoxia in IH-treated cells

We then determined whether RyRs contribute to the augmented $[Ca^{2+}]_i$ and catecholamine secretory responses to hypoxia in IH-treated chromaffin cells. At millimolar concentrations, ryanodine blocks RyRs (Takeuchi et al., 2001). Therefore, experiments were performed in a Ca^{2+}-free medium in the presence and absence of 10 mM ryanodine. Despite the Ca^{2+}-free medium containing 0.5 mM EGTA, basal $[Ca^{2+}]_i$ was still significantly higher

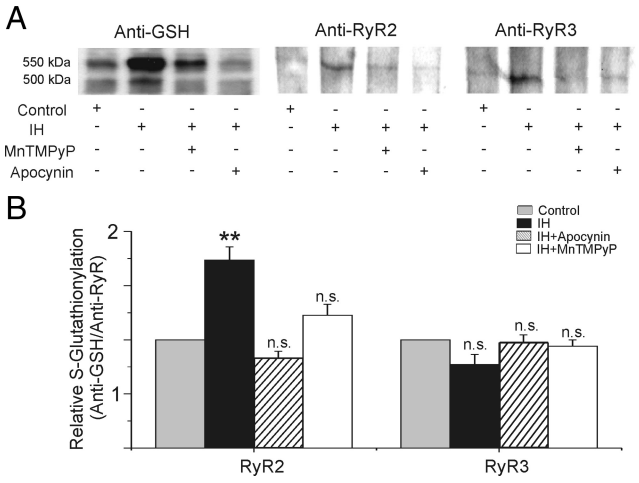

Figure 11. S-glutathionylation of RyR2 in IH-treated neonatal adrenal medullae. ***A***, Examples illustrating increased S-glutathionylation of RyR2 in IH-treated adrenal medullae and blockade of this effect by MnTMPyP or apocynin. The blot treated with anti-GSH antibody was reprobed with anti-RyR2 and RyR3 antibodies. ***B***, Average data of densitometric analysis of S-glutathionylation presented as ratio of anti-GSH/anti-RyR in normoxia-treated (control), IH-treated, IH + apocynin-treated, or MnTMPyP-treated P5 rats. Results presented as mean ± SEM from three experiments in each group. $^{**}p < 0.001$ compared with controls.

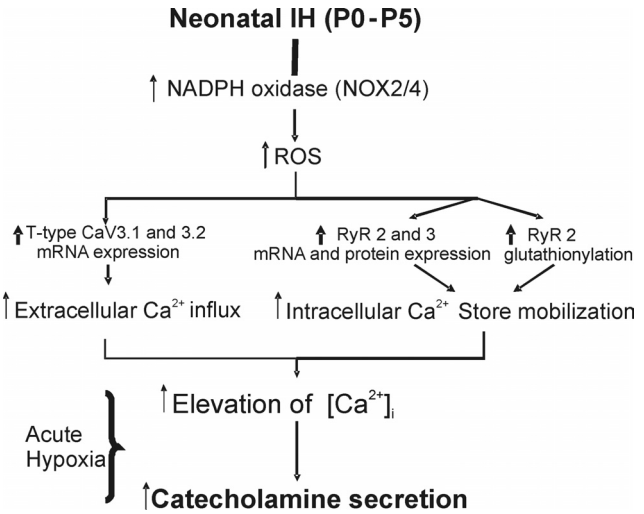

Figure 12. Schematic presentation of signaling pathways mediating the effects of IH on hypoxia-evoked catecholamine secretion in neonatal rat adrenal chromaffin cells.

in IH-treated compared with control cells (Fig. 10*A*). In the presence of 10 mM ryanodine, basal $[Ca^{2+}]_i$ levels were significantly reduced in IH-treated but not in control cells (Fig. 10*B*). More importantly, in Ca^{2+}-free medium, IH-treated cells responded to acute hypoxia with significant elevations in $[Ca^{2+}]_i$ and catecholamine secretion, and 10 mM ryanodine prevented these effects (Fig. 10*C*,*D*). In control cells, hypoxia was ineffective in elevating $[Ca^{2+}]_i$ and evoking catecholamine secretion in Ca^{2+}-free medium (data not shown).

Evidence for IH-induced redox modulation of RyRs via S-glutathionylation

The results described above suggest that IH leads to activation of RyRs under basal conditions and contribute to elevated basal $[Ca^{2+}]_i$ in IH-treated cells. Previous studies have shown that posttranslational redox modulation involving S-glutathionylation of cysteine residues activate RyRs under basal conditions (Murayama et al., 1999; Bull et al., 2008; Huddleston et al., 2008; Terentyev et al., 2008). To examine whether IH induces similar posttranslational modification of RyRs, adrenal chromaffin cell lystes were probed with anti-glutathionylated antibody and analyzed by immunoblot assay. As shown in Figure 11, *A* and *B*, IH treatment increased S-glutathionylation of RyR2 but not RyR3 compared with control cells, and this effect was abolished with systemic administration of apocynin or MnTMPyP.

Discussion

In the present study, we examined the mechanisms underlying the effects of IH on neonatal adrenal chromaffin cell responses to hypoxia. Our results demonstrated that IH treatment upregulates NOX2 and NOX4 mRNAs and apocynin, a potent inhibitor of NOX, prevented the augmented catecholamine secretion by hypoxia in IH treated cells. These findings taken together with our previous observation that O_2^- scavenger also blocks the effects of IH on hypoxia-evoked catecholamine secretion (Souvannakitti et al., 2009) demonstrate that ROS derived from the NOX family of enzymes mediate the augmented secretory responses to hypoxia in IH-treated neonatal adrenal chromaffin cells. Similar upregulation of NOX2 and NOX4 by IH was also reported in carotid bodies (Peng et al., 2009). Little is known about transcriptional regulation of NOX isoforms in general (Bedard and Krause, 2007) and hypoxia in particular. Hypoxia inducible factors HIF-1 and HIF-2 mediate transcriptional responses of several genes during hypoxia (Semenza, 2004). Whether HIFs also contribute to IH-induced upregulation of NOX2 and NOX4 remain to be investigated. Interestingly, NOX2 is localized to the cytoplasm, whereas NOX4 in the nucleus of chromaffin cells (Fig. 1), a localization pattern similar to that reported in rat carotid body glomus cells (Peng et al., 2009). However, present results show that NOX activity is constitutively increased in IH-treated neonatal chromaffin cells in contrast to the 5-HT regulated activation of NOX in IH-treated carotid bodies. Although relative roles of NOX2 and NOX4 can be best addressed by using an small interfering RNA approach, this proved to be technically difficult in primary cultures of neonatal chromaffin cells, whose viability rapidly declines with time. Nonetheless, it is conceivable that NOX4 contribution to the elevated NOX activity by IH outweighs that of NOX2 because (1)) the magnitude of NOX4 mRNA elevation was more pronounced than that of NOX2 (Fig. 1) and (2) unlike NOX2, NOX4 is constitutively active (Bedard and Krause, 2007).

Previous studies on chromaffin cells have shown that hypoxia-evoked catecholamine secretion is mediated by Ca^{2+} influx via voltage-dependent Ca^{2+} channels (Mochizuki-Oda et al., 1997). Our results with mibefradil, a blocker of T-type Ca^{2+} channels (Martin et al., 2000), suggest that Cav3.1 and Cav3.2 contribute in large part to the pronounced hypoxia-evoked Ca^{2+} influx as well as the augmented catecholamine secretion from IH-treated chromaffin cells. Mibefradil, however, had only modest effects on $[Ca^{2+}]_i$ responses and catecholamine secretion in control cells, indicating that they express a relatively small number of T-type Ca^{2+} channels. For these studies, we used a relatively high concentration of mibefradil (10 μM) to ensure complete blockade of T-type Ca^{2+} channels. Because we saw only a modest effect of mibefradil on $[Ca^{2+}]_i$ responses from control cells, our data suggest that this concentration of mibefradil was relatively selective for T-type channels. Consistent with these findings, T-type Ca^{2+} current amplitudes measured in chromaffin cells from normoxia-treated animals were modest, whereas those from IH-treated animals were more than twofold larger.

Surprisingly, we were unable to find the "shoulder" representing T-type Ca^{2+} current in every neonatal rat adrenal chromaffin cell studied. Nonetheless, there was ~20 mV separation between the activation of T-type Ca^{2+} current and other high-voltage-gated Ca^{2+} currents. Furthermore, the amplitudes of T-type Ca^{2+} current that we observed were similar to those reported by Levitsky and López-Barneo (2009). However, unlike adrenal medullary slices (Levitsky and López-Barneo, 2009), there was no spontaneous exocytosis in control or IH-treated isolated neonatal chromaffin cells. The facilitated catecholamine secretion in IH-treated chromaffin cells, conversely, support the notion put forth by Carabelli et al. (2007) that T-type Ca^{2+} couple very efficiently to exocytosis under the conditions of stress.

Although Cd^{2+} is known to block all voltage-gated Ca^{2+} channels, it is somewhat less efficient in blocking T-type Ca^{2+} channels. Complete blockade of the T-type currents may require more than the 300 μM Cd^{2+} used in the current study, which may explain the residual $[Ca^{2+}]_i$ responses observed after Cd^{2+} treatment. Indeed, our data indicate that IH leads to recruitment of additional T-type Ca^{2+} channels in neonatal adrenal chromaffin cells. Indeed, IH treatment led to marked upregulation of mRNAs encoding Cav3.1 and Cav3.2 subtypes of T-type Ca^{2+} channels, and this response requires NOX/ROS signaling because it was prevented by either a NOX inhibitor or by an O_2^- scavenger. Similar upregulation of T-type Ca^{2+} channels was also reported in response to continuous hypoxia in PC12 cells (Del Toro et al., 2003) and chromaffin cells (Carabelli et al., 2007), indicating that both IH and continuous hypoxia are potent regulators of Cav3.1 and Cav3.2 transcription. A previous study reported that HIF-2 mediates transcriptional upregulation of Cav3.2 by continuous hypoxia (Del Toro et al., 2003). However, IH downregulates HIF-2α protein in PC12 cells, adrenal medullae, and carotid bodies (Nanduri et al., 2009) but upregulates HIF-1α protein (Peng et al., 2006; Yuan et al., 2008). It is likely that HIF-1 mediates Cav3.1 and Cav3.2 upregulation in IH-treated neonatal chromaffin cells, a possibility that remains to be investigated.

Although mobilization of intracellular Ca^{2+} plays little or no role in hypoxia-evoked elevation in $[Ca^{2+}]_i$ in control neonatal adrenal chromaffin cells (Takeuchi et al., 2001), our previous study suggested mobilization of intracellular Ca^{2+} stores in IH-treated neonatal chromaffin cells (Souvannakitti et al., 2009). The following evidence suggests that RyRs mediate the hypoxia-induced mobilization of intracellular Ca^{2+} stores and contribute in part to the enhanced catecholamine secretion by hypoxia in IH-treated cells: (1) RyR1–RyR3 are expressed in neonatal chromaffin cells, (2) they are functional as evidenced by elevation of $[Ca^{2+}]_i$ in a Ca^{2+}-free medium in response to an RyR agonist, and (3) blockade of RyRs prevent hypoxia-induced elevation of $[Ca^{2+}]_i$ as well as exocytosis of catecholamines in Ca^{2+}-free medium. Our results further demonstrate that the contribution of RyRs is in part attributable to NOX/ROS-dependent transcriptional upregulation of RyR2 and RyR3 and the corresponding proteins.

Our previous study (Souvannakitti et al., 2009) as well as the current data demonstrate that basal $[Ca^{2+}]_i$ levels were elevated in IH-treated cells and this elevation persisted under Ca^{2+}-free medium, suggesting that it arises from mobilization of intracellular Ca^{2+}stores. Blockade of RyRs restored basal $[Ca^{2+}]_i$ levels in IH cells to levels seen in control cells, implying that constitutive activation of RyRs mediates the elevated basal $[Ca^{2+}]_i$ levels in IH cells. We further demonstrate that IH leads to NOX/ROS-dependent S-glutathionylation of RyR2, which is known to constitutively activate RyRs (Murayama et al., 1999; Zissimopoulos and Lai, 2006; Bull et al., 2008; Huddleston et al., 2008; Belevych et al., 2009). These observations taken together demonstrate that NOX/ROS signaling activates RyRs by transcriptional upregulation as well as by posttranslational modifications involving S-glutathionylation in IH-treated neonatal chromaffin cells resulting in constitutive activation of RyRs. The signaling mechanisms mediating the enhanced catecholamine secretion by hypoxia in IH-treated cells identified in this study are summarized in Figure 12.

Between 70 and 90% of prematurely born infants experience IH as a consequence of recurrent apneas (Stokowski, 2005). Our previous results showed that many of the IH-evoked changes in neonatal rats, including altered Ca^{2+} homeostasis in adrenal chromaffin cells, persist in juvenile life (Souvannakitti et al., 2009). Interestingly, increased Ca^{2+} entry via upregulated T-type Ca^{2+} channels has been implicated in a wide number of pathologies, including epilepsy, pain, and hypertension (Khosravani and Zamponi, 2006; Nelson et al., 2006; Powell et al., 2009). Consequently, it will be of considerable interest in the future to investigate whether upregulation of T-type Ca^{2+} channels and/or RyRs by neonatal IH persists in juvenile life and thus contributes to the altered Ca^{2+} homeostasis and the ensuing long-term pathologic consequences of neonatal IH.

References

Alonso MT, Barrero MJ, Michelena P, Carnicero E, Cuchillo I, García AG, García-Sancho J, Montero M, Alvarez J (1999) Ca^{2+}-induced Ca^{2+} release in chromaffin cells seen from inside the ER with targeted aequorin. J Cell Biol 144:241–254.

Bedard K, Krause KH (2007) The NOX family of ROS-generating NADPH oxidases: physiology and pathophysiology. Physiol Rev 87:245–313.

Belevych AE, Terentyev D, Viatchenko-Karpinski S, Terentyeva R, Sridhar A, Nishijima Y, Wilson LD, Cardounel AJ, Laurita KR, Carnes CA, Billman GE, Gyorke S (2009) Redox modification of ryanodine receptors underlies calcium alternans in a canine model of sudden cardiac death. Cardiovasc Res 84:387–395.

Bull R, Finkelstein JP, Gálvez J, Sánchez G, Donoso P, Behrens MI, Hidalgo C (2008) Ischemia enhances activation by Ca^{2+} and redox modification of ryanodine receptor channels from rat brain cortex. J Neurosci 28:9463–9472.

Carabelli V, Marcantoni A, Comunanza V, de Luca A, Díaz J, Borges R, Carbone E (2007) Chronic hypoxia up-regulates alpha1H T-type channels and low-threshold catecholamine secretion in rat chromaffin cells. J Physiol 584:149–165.

Colliver TL, Pyott SJ, Achalabun M, Ewing AG (2000) VMAT-mediated changes in quantal size and vesicular volume. J Neurosci 20:5276–5282.

Del Toro R, Levitsky KL, López-Barneo J, Chiara MD (2003) Induction of T-type calcium channel gene expression by chronic hypoxia. J Biol Chem 278:22316–22324.

Huddleston AT, Tang W, Takeshima H, Hamilton SL, Klann E (2008) Superoxide-induced potentiation in the hippocampus requires activation of ryanodine receptor type 3 and ERK. J Neurophysiol 99:1565–1571.

Khosravani H, Zamponi GW (2006) Voltage-gated calcium channels and idiopathic generalized epilepsies. Physiol Rev 86:941–966.

Kuri BA, Chan SA, Smith CB (2009) PACAP regulates immediate catecholamine release from adrenal chromaffin cells in an activity-dependent manner through a protein kinase C-dependent pathway. J Neurochem 110:1214–1225.

Lagercrantz H, Bistoletti P (1977) Catecholamine release in the newborn infant at birth. Pediatr Res 11:889–893.

Levitsky KL, López-Barneo J (2009) Developmental change of T-type Ca^{2+} channel expression and its role in rat chromaffin cell responsiveness to acute hypoxia. J Physiol 587:1917–1929.

Marengo JJ, Bull R, Hidalgo C (1996) Calcium dependence of ryanodine-sensitive calcium channels from brain cortex endoplasmic reticulum. FEBS Lett 383:59–62.

Martin RL, Lee JH, Cribbs LL, Perez-Reyes E, Hanck DA (2000) Mibefradil block of cloned T-type calcium channels. J Pharmacol Exp Ther 295:302–308.

Mayo LA, Curnutte JT (1990) Kinetic microplate assay for superoxide production by neutrophils and other phagocytic cells. Methods Enzymol 186:567–575.

Mochizuki-Oda N, Takeuchi Y, Matsumura K, Oosawa Y, Watanabe Y (1997) Hypoxia-induced catecholamine release and intracellular Ca^{2+} increase via suppression of K^+ channels in cultured rat adrenal chromaffin cells. J Neurochem 69:377–387.

Murayama T, Oba T, Katayama E, Oyamada H, Oguchi K, Kobayashi M, Otsuka K, Ogawa Y (1999) Further characterization of the type 3 ryanodine receptor (RyR3) purified from rabbit diaphragm. J Biol Chem 274:17297–17308.

Nanduri J, Wang N, Yuan G, Khan SA, Souvannakitti D, Peng YJ, Kumar GK, Garcia JA, Prabhakar NR (2009) Intermittent hypoxia degrades HIF-2alpha via calpains resulting in oxidative stress: implications for recurrent apnea-induced morbidities. Proc Natl Acad Sci U S A 106:1199–1204.

Nelson MT, Todorovic SM, Perez-Reyes E (2006) The role of T-type calcium channels in epilepsy and pain. Curr Pharm Des 12:2189–2197.

Pawar A, Peng YJ, Jacono FJ, Prabhakar NR (2008) Comparative analysis of neonatal and adult rat carotid body responses to chronic intermittent hypoxia. J Appl Physiol 104:1287–1294.

Peng YJ, Yuan G, Jacono FJ, Kumar GK, Prabhakar NR (2006) 5-HT evokes sensory long-term facilitation of rodent carotid body via activation of NADPH oxidase. J Physiol 576:289–295.

Peng YJ, Nanduri J, Yuan G, Wang N, Deneris E, Pendyala S, Natarajan V, Kumar GK, Prabhakar NR (2009) NADPH oxidase is required for the sensory plasticity of the carotid body by chronic intermittent hypoxia. J Neurosci 29:4903–4910.

Powell KL, Cain SM, Ng C, Sirdesai S, David LS, Kyi M, Garcia E, Tyson JR, Reid CA, Bahlo M, Foote SJ, Snutch TP, O'Brien TJ (2009) A Cav3.2 T-type calcium channel point mutation has splice-variant-specific effects on function and segregates with seizure expression in a polygenic rat model of absence epilepsy. J Neurosci 29:371–380.

Randall AD, Tsien RW (1997) Contrasting biophysical and pharmacological properties of T-type and R-type calcium channels. Neuropharmacology 36:879–893.

Sánchez G, Pedrozo Z, Domenech RJ, Hidalgo C, Donoso P (2005) Tachycardia increases NADPH oxidase activity and RyR2 S-glutathionylation in ventricular muscle. J Mol Cell Cardiol 39:982–991.

Seidler FJ, Slotkin TA (1985) Adrenomedullary function in the neonatal rat: responses to acute hypoxia. J Physiol 358:1–16.

Semenza GL (2004) O2-regulated gene expression: transcriptional control of cardiorespiratory physiology by HIF-1. J Appl Physiol 96:1173–1177; discussion 1170–1172.

Simpson PB, Challiss RA, Nahorski SR (1995) Neuronal Ca^{2+} stores: activation and function. Trends Neurosci 18:299–306.

Souvannakitti D, Kumar GK, Fox A, Prabhakar NR (2009) Neonatal intermittent hypoxia leads to long-lasting facilitation of acute hypoxia-evoked catecholamine secretion from rat chromaffin cells. J Neurophysiol 101:2837–2846.

Stokowski LA (2005) A primer on apnea of prematurity. Adv Neonatal Care 5:155–170; quiz 171–174.

Takeuchi Y, Mochizuki-Oda N, Yamada H, Kurokawa K, Watanabe Y (2001) Nonneurogenic hypoxia sensitivity in rat adrenal slices. Biochem Biophys Res Commun 289:51–56.

Terentyev D, Györke I, Belevych AE, Terentyeva R, Sridhar A, Nishijima Y, de Blanco EC, Khanna S, Sen CK, Cardounel AJ, Carnes CA, Györke S (2008) Redox modification of ryanodine receptors contributes to sarcoplasmic reticulum Ca^{2+} leak in chronic heart failure. Circ Res 103:1466–1472.

Yuan G, Nanduri J, Khan S, Semenza GL, Prabhakar NR (2008) Induction of HIF-1alpha expression by intermittent hypoxia: involvement of NADPH oxidase, Ca^{2+} signaling, prolyl hydroxylases, and mTOR. J Cell Physiol 217:674–685.

Zhan G, Serrano F, Fenik P, Hsu R, Kong L, Pratico D, Klann E, Veasey SC (2005) NADPH oxidase mediates hypersomnolence and brain oxidative injury in a murine model of sleep apnea. Am J Respir Crit Care Med 172:921–929.

Zissimopoulos S, Lai FA (2006) Redox regulation of the ryanodine receptor/calcium release channel. Biochem Soc Trans 34:919–921.